Journal of Materials Chemistry A

Accepted Manuscript

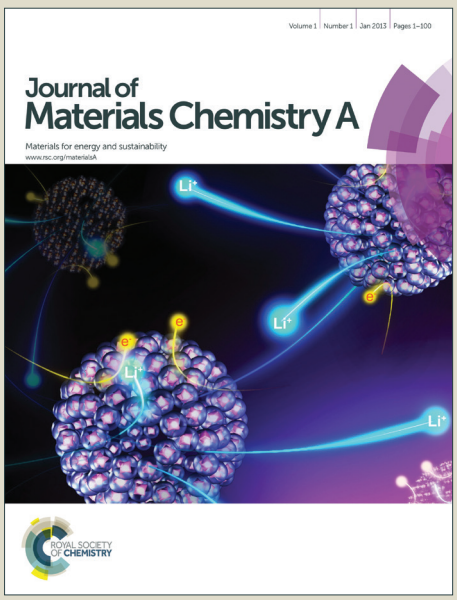

ROYAL SOCIETY OF CHEMISTRY

www.rsc.org/materialsA

An electrochemical sensing platform based on reduced graphene oxide-cobalt oxide nanocubes@platinum nanocomposite for nitric oxide detection

Muhammad Mehmood Shahid[1], Perumal Rameshkumar[1], Alagarsamy Pandikumar[1], Hong Ngee Lim[2,3], Yun Hau Ng[4], Nay Ming Huang[1]*

[1]Low Dimensional Materials Research Centre, Department of Physics, Faculty of Science, University of Malaya, 50603 Kuala Lumpur, Malaysia

[2] Department of Chemistry, Faculty of Science, University Putra Malaysia, 43400 UPM Serdang, Selangor, Malaysia

[3]Functional Device Laboratory, Institute of Advanced Technology, University Putra Malaysia, 43400 UPM Serdang, Selangor, Malaysia

[4]Particles and Catalysis Research Group, School of Chemical Engineering, The University of New South Wales, Sydney NSW 2052, Australia

Corresponding author:
huangnayming@um.edu.my

Abstract

We report a facile one-pot hydrothermal synthesis of reduced graphene oxide-cobalt oxide nanocubes@platinum (rGO-Co_3O_4@Pt) nanocomposite and its application toward the electrochemical detection of nitric oxide (NO). The rGO-Co_3O_4@Pt nanocomposite was characterized by field emission scanning electron microscopy (FESEM), energy dispersive X-ray (EDX) mapping, X-ray diffraction (XRD) and Raman analyses. The nanocomposite modified glassy carbon (GC) electrode was used for the electrochemical oxidation of nitric oxide (NO) and it showed better catalytic performance in terms of catalytic peak current and shift in overpotential when compared to rGO, Co_3O_4 nanocubes and rGO-Co_3O_4 nanocomposite modified electrodes. The rGO-Co_3O_4@Pt nanocomposite modified electrode showed a better sensing ability toward the in-situ generated NO in NO_2^- containing phosphate buffer solution (PBS) than the other controlled modified electrodes. The Pt nanoparticles present in the nanocomposite could enhance the sensing performance and the limit of detection (LOD) was found as 1.73 μM with signal-to-noise (S/N) ratio ~3 using amperometric i-t curve. Further, the nanocomposite modified electrode showed the selectivity toward the detection of NO in the presence of 100-fold higher concentration of other physiologically important analytes. The proposed sensor was stable, reproducible and selective toward the detection of NO.

Keywords: Reduced graphene oxide; Cobalt oxide nanocubes; Platinum nanoparticles; Electrochemical sensor; Nitric oxide.

1. Introduction

Nitric oxide (NO) is one of the smallest and simplest biologically important molecules in nature with distinctive and fascinating chemistry.[1] Ignarro, Furchgott and Murad identified NO as endothelium-derived relaxation factor (EDRF) which is responsible for vasodilation and blood pressure regulation in the nervous and cardiovascular systems of mammalian physiology.[2-5] NO plays extremely important physiological roles as an endogenously-produced antimicrobial agent,[6] as a signalling molecule capable of modulating cytokine production[7] and also, it plays a key role in wound healing[8] and in immune response.[9] The multi-tasking NO is actually produced endogenously by a class of heme-containing enzymes called nitric oxide synthases.[10, 11] Due to the extensive interest in NO regarding biochemical as well as a medical perspective, it is vitally important to monitor the concentration level of NO in physiological system very closely. The concentration of NO varies in human body from sub-nanomolar to micromolar levels.[12] Some parameters are very important for the effective detection of NO such as adequate sensitivity, fast response time, wide dynamic range, and high selectivity toward NO over interfering species. Due to the irresistible complexity of biological systems, these parameters are often challenging. Besides all the mentioned challenges, the chemical properties of NO make the detection very complex. Fortunately, some analytical techniques including spectroscopic and electrochemical methods are often used for the detection of NO. Among the various methods, electrochemical method is an efficient analytical technique to detect NO because of its long term high calibration stability, fast response, good sensitivity, better selectivity and simplicity.[13]

In recent years, constructing a competent electrochemical sensor is highly motivated among researchers for the sensitive detection of NO. Recently, efforts have been made to increase the sensitivity for electrochemical detection of NO by engineering the electrode with

functional nanomaterials.[12, 14] Different type of nanomaterials including single-walled carbon nanotubes (SWCNTs)[15], multi-walled carbon nanotubes (MWCNTs)[16], nano-alumina[17], Nafion-nickel (II) porphyrin film[18] and gold nanoparticles[19] etc. have been previously used for the detection of NO. Graphene based nanocomposite materials as electrochemical sensors have also been reported for the detection of NO.[20-22] As known, graphene is a two dimensional carbon sheet having single atom thickness, large theoretical surface area (2630 m^2 g^{-1}) with high conductivity at room temperature (10^6 s cm^{-1}) and wide electrochemical window.[23, 24] Graphene nanosheet is an excellent host material for growing nanomaterials for the high performance electrochemical applications.[25, 26] To date, a large number of graphene based nanocomposite materials has been synthesized for different applications like energy storage[27], biosensor[28] and electrocatlaytic[29] applications etc. A number of reports are available for hosting a variety of metals, metal oxides and semiconductor nanoparticles on graphene nanosheets and their various electrocatalytic applications have been reported.[30-33] Among the library of many transition metal oxides, cobalt oxide (Co_3O_4) got much attention by the researchers due to its high surface area to volume ratio, high ratio of surface atoms and good chemical stability and it is expected to meet the requirements of future energy applications.[34] Owing these properties, unaided Co_3O_4 nanoparticles have been used in many reports for variety of applications[35-38]. However, only few attempts have been made to synthesize graphene-cobalt oxide nanocomposite and used for electrocatalytic applications.[28,39,40] For the synthesis of graphene–metal oxide nanocomposites, hydrothermal synthesis is highly preferred because an appropriate amount of powdered reagents and water are placed in a Teflon-lined autoclave and heated without stirring from moderate to high temperatures and pressures for the desired time and the possibility of predicting optimum reaction conditions by electrolyte thermodynamics.[41]

In this work, we report an electrochemical sensing platform based on one-pot hydrothermally synthesized rGO-Co_3O_4@Pt nanocomposite for the detection of in-situ generated NO. The formation of rGO-Co_3O_4@Pt nanocomposite was confirmed by FESEM, EDX mapping, XRD and Raman analyses. The rGO-Co_3O_4@Pt nanocomposite modified glassy carbon (GC) electrode displayed better catalytic performance toward the oxidation of NO when compared to the other controlled modified electrode investigated in this work. The detection of lower concentration of NO was studied using amperometric i-t curve technique and the LOD was found as 1.73 μM with signal-to-noise (S/N) ratio ~3. The use of less concentration of Pt improved the sensitivity of the rGO-Co_3O_4@Pt nanocomposite modified electrode. Moreover, the nanocomposite modified electrode was stable, reproducible and showed an excellent selectivity toward the detection of NO in the presence of 100-fold higher concentration of other physiologically important interferents.

2. Experimental methods

2.1. Materials

Graphite flakes was purchased from Asbury Inc. (USA). Potassium permanganate ($KMnO_4$, >99 %), sulphuric acid (H_2SO_4, 98%), hydrochloric acid (HCl, 35 %), and ammonia solution (NH_3, 25%) were received from R & M Chemicals. Cobalt acetate tetrahydrate ($Co(CH_3COO)_2.4H_2O$) and potassium tetrachloroplatinate(II) (K_2PtCl_4) were obtained from Sigma Aldrich and Acros Organics, respectively. Hydrogen peroxide (H_2O_2) and sodium nitrite ($NaNO_2$) were obtained from Systerm and Merck, respectively. All the chemicals used in this study were of analytical grade. Doubly distilled water was used to prepare the solutions for all the experiments.

2.2. Synthesis of rGO-Co_3O_4@Pt nanocomposite

First, GO was prepared by following the simplified Hummer's method.[42] For the preparation of rGO-Co_3O_4@Pt nanocomposite, 12 mL of 1 mmol of $Co(CH_3COO)_2.4H_2O$ solution was mixed with GO solution (8 wt.%) and stirred for 1.5 h to get a homogeneous solution. To this solution, 1 mL of 10 mM K_2PtCl_4 was added slowly under stirring and after that, 15 mL of 7.5 % ammonia was added drop-wise into the above reaction mixture under vigorous stirring. Then, 75 mL of the reaction mixture was transferred to a 100 mL Teflon-lined stainless steel autoclave for hydrothermal treatment at 180 °C for 12 h. After hydrothermal treatment, the precipitate of rGO-Co_3O_4@Pt nanocomposite was washed five times with deionized water and ethanol and dried in a hot air oven at 60 °C. The solid product of the nanocomposite was collected and used for further studies. The synthesis of rGO, Co_3O_4 nanocubes and rGO-Co_3O_4 nanocomposite were followed by using a similar method. For the optimization of GO, rGO-Co_3O_4 nanocomposite was prepared using different amounts of GO (4 and 12%). The rGO-Co_3O_4 nanocomposite used in this work contains 8 wt.% of GO, unless otherwise mentioned.

2.3. Electrochemical measurements

The rGO-Co_3O_4@Pt nanocomposite modified glassy carbon (GC) electrode was fabricated by dissolving the nanocomposite in doubly distilled water (1 mg/mL) and drop-casting 5 μL of the nanocomposite solution on GC electrode (d = 3 mm) surface and allowed to dry at room temperature (25 ^oC) for 2 h. The so fabricated GC was used as a working electrode. Prior to the modification, GC electrode was polished with 0.05 micron alumina slurry and cleaned by potential cycling between +1 and -1 V in 0.1 M H_2SO_4 before the experiments. All the electrochemical studies were carried out under nitrogen atmosphere using VersaSTAT-3

electrochemical analyser (Princeton Applied Research, USA) with conventional three-electrode system. Platinum (Pt) wire and Ag/AgCl were used as counter and reference electrodes, respectively. Phosphate buffer solution (PBS) (pH 2.5) was used as supporting electrolyte and $NaNO_2$ was used as precursor to generate the NO in solution.

2.4. Characterization techniques

Morphology and elemental mapping analysis including energy dispersive X-ray (EDX) spectrum of rGO-Co_3O_4@Pt nanocomposite were studied by using JEOL JSM-7600F field emission scanning electron microscopy fitted with EDX and elemental mapping. The crystalline nature of the nanocomposite was analysed by using Philips X'pert X-ray diffractometer with copper Kα radiation (λ=1.5418 nm) at a scan rate of 0.02 degree-sec^{-1}. Raman spectra was obtained by using Renishaw inVia 2000 system green laser emitting at 514 nm.

3. Results and discussion

3.1. Morphological characterization of rGO-Co_3O_4@Pt nanocomposite

FESEM analysis was performed to study the morphology of the rGO-Co_3O_4@Pt nanocomposite (Fig. 1). The FESEM image of rGO (Fig. 1a) shows the sheet like structure and Co_3O_4 formed as cubical nanostructures (Fig. 1b). After the formation of rGO-Co_3O_4 composite, Co_3O_4 nanocubes retained their morphology and well deposited and distributed on the rGO sheets (Fig. 1c). While some of the Co_3O_4 nanocubes are present in between the rGO sheets and displayed as blurred images some of the nanocubes are located on the surface of the rGO sheets and exposed as clear images. The morphology of rGO-Co_3O_4 composite with different concentrations of GO (4 and 12 wt.%) was also evaluated and they also displayed the formation well stabilized cubical Co_3O_4 nanostructures on the rGO sheets (Fig. S1). The use of ammonia facilitated the precipitation of cobalt ions and the reduction of GO. The Co_3O_4 nanocubes can be

strongly anchored onto the rGO matrix due to the interaction between Co_3O_4 and rGO through interfacial Co-O-C bonds formed by the high reactivity of SP^2 carbon atom of rGO with electron-rich oxygen species of Co_3O_4.[43] During the formation of rGO-Co_3O_4@Pt nanocomposite, Pt nanoparticles are densely decorated on Co_3O_4 without altering the cubical structure of Co_3O_4 and the surface of Co_3O_4 nanocubes became rough after the deposition of Pt (Fig. 1d). Further, it is understood from the FESEM image of the nanocomposite that rGO sheets prevent Co_3O_4 nanocubes from agglomeration and Co_3O_4@Pt behaves like a spacer between rGO sheets.[44] The FESEM image of the rGO-Co_3O_4@Pt nanocomposite reveals an efficient decoration of Pt nanoparticles on Co_3O_4 nanocubes in rGO matrix using hydrothermal synthesis.

The distribution of elements present in the rGO-Co_3O_4@Pt nanocomposite was studied by EDX elemental mapping analysis (Fig. 2). The EDX spectrum of rGO-Co_3O_4@Pt nanocomposite shows the signatures of elemental O (33.89 wt.%), Co (50.43 wt.%), C (14.74 wt.%) and Pt (0.94 wt.%) and thereby confirms the presence of the same in the nanocomposite (Fig. S2). Figure 2a shows the FESEM image of the nanocomposite and the elements O (black color), Co (green color), C (blue color) and Pt (red color) were scanned as shown in the EDX mapping profile of rGO-Co_3O_4@Pt nanocomposite (Fig. 2b). The independent elemental O, Co, C and Pt distributions are shown in Fig. 2(c-f) and it displays a clear distribution of Pt nanoparticles on Co_3O_4 nanocubes. The large area coverage of black (Fig. 2c), green (Fig. 2d) and blue (Fig. 2e) colors indicates the dense package of Co_3O_4 nanocubes in between the rGO sheets and on the surface of rGO sheets. Figure 2f shows the elemental distribution of Pt on the surface of Co_3O_4 nanocubes and some area of the image seems to be empty due to the unexposed Co_3O_4@Pt nanocubes.

3.2. XRD and Raman analyses

The crystalline nature of the rGO-Co_3O_4@Pt nanocomposite was evaluated by XRD analysis (Fig. 3). The diffraction peaks observed at 31.2°, 36.8°, 44.7°, 55.5°, 59.2°, 65.1° and 77.2° correspond to (2 2 0), (3 1 1), (4 0 0), (4 2 2), (4 4 0), (5 1 1) and (5 3 3) crystal planes of face centered cubic Co_3O_4 (JCPDS Card No. 42-1467).[45] The observed 2θ values are in good agreement with the standard database values. The diffraction peaks of Pt nanoparticles might associate with noise and the intense Co_3O_4 diffraction peaks might mask the peaks of Pt since a small amount of Pt was used in the synthesis of rGO-Co_3O_4@Pt nanocomposite. Pt possesses 2θ values of 39.2°, 45.6°, 66.5° and 80.1° corresponding to (1 1 1), (2 0 0), (2 2 0) and (3 1 1) crystal planes (JCPDS Card No. 88-2343) and these 2θ values are closer to those of Co_3O_4. No distinguishable peak was observed for the carbon diffraction of rGO because of very thin layer of rGO sheet.

Raman spectroscopy is used as a conventional tool to monitor the structural change of graphene-based materials. Figure 4 displays the Raman spectra of GO, rGO sheet and rGO-Co_3O_4-Pt nanocomposite. The Raman spectra of both GO (Fig. 4A(inset)) and rGO showed the two intense distinguishable peaks at 1356 and 1588 cm^{-1} corresponding to D and G bands, respectively (Fig. 4A). D band is ascribed to the lattice defect induced phonon mode and G band refers to the C-C bond expansion or contraction in hexagonal carbon plane.[46,47] The degree of disorder and the average size of the in-plane sp^2 domains are specified by the intensity ratio of the D to G bands (I_D/I_G).[46] The I_D/I_G of rGO was estimated as 1.02, which is higher than that of GO (0.88), suggesting the formation of partially ordered crystal structures and the decreased size of in-plane sp^2 domains during the reduction of GO.[46] It is known that 2D band is valuable to differentiate the monolayer from multi-layer sheets in graphene based material. It can be seen

that the slight increase in the 2D band intensity in rGO than GO which suggests the formation of exfoliated rGO sheets from the densed multilayer GO sheets. The Raman spectrum of rGO-Co_3O_4@Pt nanocomposite retained almost the same value of I_D/I_G for rGO with the 2D peak (Fig. 4B) and the peaks appeared at 476, 522, 616 and 683 cm^{-1} are attributed to the E_g, F_{2g}^1, F_{2g}^2 and A_{1g} modes of Co_3O_4, respectively (Fig. 4B(inset)).[48, 49]

3.3. Electrochemistry of the redox marker $[Fe(CN)_6]^{3-/4-}$ and electrochemical impedance spectroscopy analysis

The redox behavior of $[Fe(CN)_6]^{3-/4-}$ couple is a valuable tool to study the kinetic barrier of the electrode-solution interface since the electron-transfer between the electroactive species in solution and the electrode surface occurs by tunneling of electrons either through the barrier or through the defects or pinholes present in the barrier.[50] Figure 5 explains the comparison of cyclic voltammetric responses obtained at the bare GC, Co_3O_4 nanocubes, rGO, rGO-Co_3O_4 nanocomposite and rGO-Co_3O_4@Pt nanocomposite modified electrodes for 1 mM $K_3[Fe(CN)_6]$ in 0.1 M KCl at a scan rate of 50 mV s^{-1}. As known, bare GC electrode shows a reversible votammetric characteristic for the one electron redox process of $[Fe(CN)_6]^{3-/4-}$ couple with the peak-to-peak separation of 63 mV and with oxidative peak area of 24.016 µC at a scan rate of 50 mV s^{-1}. The Co_3O_4 nanocubes modified electrode shows the enhanced redox peak currents with oxidative peak area of 27.176 µC when compared to bare GC and because of high conductivity of rGO sheets the electron transfer kinetics was more facilitated at rGO modified electrode and thereby showed a higher peak current with oxidative peak area of 20.046 µC. The occurrence of facile electron transfer at the rGO-Co_3O_4 nanocomposite modified electrode surface was understood by the enhanced peak current with oxidative peak area of 27.640 µC when compared to the Co_3O_4 nanocubes and rGO modified electrodes. The rGO-Co_3O_4@Pt nanocomposite

modified electrode retained the reversible voltammetric response for the $[Fe(CN)_6]^{3-/4-}$ couple and showed higher redox peak currents with oxidative peak area of 31.884 μC among all the modified electrodes investigated in this work. The redox peak current of rGO-Co_3O_4 nanocomposite was further enhanced by the presence of Pt nanoparticles in the rGO-Co_3O_4@Pt nanocomposite modified electrode. This observation clearly reveals that the rGO-Co_3O_4@Pt nanocomposite acts as a new electrode surface with increased electrode area and Co_3O_4@Pt has good electrical communication with the underlying electrode surface through rGO sheets.

The interfacial properties of surface-modified electrodes were studied by the electrochemical impedance spectroscopy (EIS).[51] The $[Fe(CN)_6]^{3-/4-}$ couple was used as a redox analyte to study the conducting behavior of the rGO-Co_3O_4@Pt nanocomposite modified electrode. The Nyquist diagram of the complex impedance represents the imaginary versus the real part of the impedance and it shows the semicircle at higher frequencies corresponding to the electron transfer-limited process and the linear portion at lower frequencies corresponding to the diffusion-limited process.[52] The EIS responses were recorded for 1 mM $[Fe(CN)_6]^{3-/4-}$ in 0.1 M KCl at all the modified electrodes (Fig. 6). Bare GC electrode showed a semicircle-like shape Nyquist plot with large diameter which suggests the hindrance to the electron-transfer kinetics at the electrode surface (Fig. 6a). When the electrode was modified with Co_3O_4 nanocubes (Fig. 6b) and rGO (Fig. 6c) the electron transfer resistance (R_{ct}) values were decreased from 38400 Ω to 11300 Ω and from 38400 Ω to 830 Ω, respectively. The rGO-Co_3O_4 nanocomposite modified electrode showed only the linear portion at lower frequencies indicating the diffusion-limited process at the electrode-solution interface (Fig. 6d). The diffusion-limited process much more facilitated at the rGO-Co_3O_4@Pt nanocomposite modified electrode due to the conducting behavior of Pt present in the nanocomposite (Fig. 6e). A perfect linear portion was observed at

lower frequencies for the rGO-Co_3O_4@Pt nanocomposite modified electrode when compared to the rGO-Co_3O_4 nanocomposite modified electrode. These results indicate that the rGO-Co_3O_4@Pt nanocomposite was successfully formed and it facilitated a diffusion-limited process at the electrode-solution interface. Bode-phase plots of the modified electrodes were collected in the frequency range of 0.01–10000 Hz (Fig. S3A). The phase peaks appeared at a frequency range of 100–1000 Hz correspond to the charge-transfer resistance of the modified electrodes. The shifting of peaks toward the low frequency region of 0.1–100 Hz for the rGO-Co_3O_4 and rGO-Co_3O_4@Pt nanocomposite modified electrodes indicates the fast electron-transfer behavior of the nanocomposites. The conducting nature of Pt present in the rGO-Co_3O_4@Pt nanocomposite modified electrode facilitates the peak shift in Bode plot. The phase angle of the rGO-Co_3O_4@Pt nanocomposite modified electrode is much less than 90° at higher frequencies which suggests that the electrode does not behave like an ideal capacitor.[53] Bode impedance plot of rGO-Co_3O_4@Pt nanocomposite modified electrode showed a lesser log Z value at a low frequency range of 1-100 Hz in logarithm when compared to the other modified electrodes (Fig. S3B).

3.4. Electrocatalysis of nitric oxide (NO)

The electrocatlytic oxidation of NO was carried out in 0.1 M PBS (pH 2.5). $NaNO_2$ was used as precursor to produce NO in PBS to study the electrocatalytic activity of the rGO-Co_3O_4@Pt nanocomposite modified electrode. In acidic solution (pH<4), $NaNO_2$ can generate NO by the disproportionation reaction (eq 1).[19,54] Addition of a known amount of $NaNO_2$ into the bulk electrolyte solution at pH<4 generates a series of concentrations of NO.[19]

$$3HONO \longrightarrow H^+ + 2NO + NO_3^- + H_2O \quad \text{---------- (1)}$$

Figure 7 displays the cyclic voltammetric responses of the modified electrodes used in this work for the oxidation of NO in 0.1 PBS (pH 2.5) containing 5 mM NO_2^- ions. The rGO-Co_3O_4@Pt nanocomposite modified GC electrode showed catalytic NO oxidation peak at +0.84 V in 0.1 M PBS containing 5 mM of NO_2^- at a scan rate of 50 mV s^{-1} (Fig. 7f). However, the nanocomposite modified electrode did not show any voltammetric response in the absence of NO_2^- (Fig. S4a). The Co_3O_4 nanocubes (Fig. 7b) and rGO sheet (Fig. 7c) modified electrodes showed the oxidation peak for NO at almost same potential (~ +0.95 V) with less difference in the peak current. The rGO-Co_3O_4 nanocomposite modified electrode shifted the oxidation peak potential of NO (+0.87 V) towards less positive potential with a small enhancement in the peak current (Fig. 7d). For comparison, the rGO-Pt nanocomposite modified electrode was also fabricated and it showed a peak current of 102 μA at the peak potential of +0.87 V for NO oxidation (Fig. 7e). From these results, it can be concluded that the rGO-Co_3O_4@Pt nanocomposite modified electrode displayed a synergistic catalytic effect of Co_3O_4 nanocubes and Pt nanostructures toward NO oxidation. Co_3O_4 nanocubes provided a large surface area for Pt deposition and thereby enhanced the electrocatalytic activity of rGO-Co_3O_4@Pt nanocomposite modified electrode. The rGO-Co_3O_4@Pt nanocomposite modified GC electrode efficiently shifted the catalytic peak potential of NO with a peak current of 119 μA when compared to the other controlled modified electrodes investigated in this work. This reveals that Pt nanoparticles present in the nanocomposite are in good electrical communication with rGO-Co_3O_4 which resulting an efficient electron-transfer process at the modified electrode toward NO oxidation. The Pt nanoparticles also provide a larger surface area for the effective interaction of NO and thereby improved the electron-transfer kinetics and the electrocatalytic performance. The NO oxidation at the rGO-Co_3O_4@Pt nanocomposite modified electrode possibly proceeds through an

electrochemical reaction followed by a chemical reaction.[15] During the electrochemical oxidation of NO, one electron from the NO molecule transfers to the electrode with the formation of nitrosonium ion (NO^+).[15] Bare GC electrode also displayed a voltammetric response for the oxidation of NO at +0.94 V with lesser peak current (79 μA) than the other modified electrodes (Fig. 7a). The electrocatalytic oxidation of NO was performed using rGO-Co_3O_4 nanocomposite containing different amounts of GO (4, 8 and 12 wt.% GO) (Fig. S5). The rGO-Co_3O_4 nanocomposite prepared using 8 wt.% GO showed better performance toward the oxidation of NO and it was preferred to synthesize the rGO-Co_3O_4@Pt nanocomposite. The reproducibility and repeatability of the nanocomposite modified electrode were checked by recording the voltammograms with different electrodes and good reproducible and repeatable results were observed. The stability of the nanocomposite modified electrode was studied for NO oxidation by recording the voltammogram of the same modified electrode after one week and the electrode showed only less than 5% decrement in the peak current. The modified electrode was stored at room temperature (25 °C) during the period of stability measurements. This infers that the present nanocomposite modified electrode was stable towards the electrocatalytic oxidation of NO.

The cyclic voltammograms were recorded at the rGO-Co_3O_4@Pt nanocomposite modified electrode for different concentrations of NO_2^- in 0.1 M PBS (pH 2.5) and the voltammetric curves are displayed in Fig. 8. The anodic peak current for the oxidation of NO_2^- increased with increasing concentration of NO_2^- and the plot of peak current versus concentration of NO_2^- showed a linear response (Fig. 8 (inset 'A')). The plot of $\log(I_{pa})$ versus $\log[NO_2^-]$ showed a linear graph with a slope value approximately equal to 1, which indicates that the electrooxidation of NO follows first order kinetics with respect to NO_2^- concentration at the rGO-

Co_3O_4@Pt nanocomposite modified electrode (Fig. 8 (inset 'B')). The cyclic voltammograms were recorded for the oxidation of NO with different scan rates and the peak current for NO oxidation was found to be linear with square root of scan rate ($\nu^{1/2}$) (Fig. S6A) and the linear relation indicates the elctrocatalytic oxidation of NO at the nanocomposite modified electrode is controlled by the diffusion process.[55] A gradual increase in the oxidation peak potentials (E_{pa}) with increasing the scan rate (ν) indicates the chemical irreversibility of electrocatalytic NO oxidation process at the nanocomposite modified electrode. The irreversible electrooxidation of NO is also supported by the linear relation between peak potential (E_p) and log(ν) (Fig. S6B).[56] The diffusion coefficient (D) of NO was determined for the nanocomposite modified electrode by using Cottrell equation (eqn. 2).

$$I = nFD^{1/2}AC_0\pi^{-1/2}t^{-1/2} \qquad \text{---------- (2)}$$

Where n is the number of transferred per NO molecule during oxidation, F is the Faraday constant, C_0 is the concentration of NO_2^-, A is the geometric area of the electrode and t is time. The chronoamperograms were recorded at the nanocomposite modified electrode for different concentrations of nitrite ions (Fig. S7A) and the plot of peak current versus $t^{-1/2}$ showed a linear relationship (Fig. S7B). The slopes of the obtained linear lines were plotted against the NO_2^- concentrations (Fig. S7B (inset)) and from this plot, D was calculated as 3.8×10^{-5} cm^2 s^{-1}.

3.5. Amperometric detection of NO

Amperometric i-t curve technique is used as an important analytical tool for the detection of low concentration of analytes and it is a convenient technique to perform the interference study. The sensing ability of all the modified electrodes used in this work was investigated one by one for the successive addition of 1 mM of NO_2^- ions in a homogeneously stirred solution of 0.1 M PBS at a regular time interval of 60 s (Fig. 9). All the modified electrodes produced

current responses for the injection of NO_2^- ions (Fig. 9A) and among them, the rGO-Co_3O_4@Pt modified electrode showed the highest response for the every injection of NO_2^- ions with good linear range of 1 mM-14 mM (Fig. 9B). The presence of Pt anoparticles on the electrode effectively enhanced the sensing ability of the rGO-Co_3O_4@Pt nanocomposite toward the detection of NO. The rGO-Co_3O_4@Pt nanocomposite was chosen as an electrochemical sensor material for the detection of lower concentration levels of NO in PBS. The amperometric i-t curve was obtained at rGO-Co_3O_4@Pt modified electrode for the successive addition of NO_2^- ions with different concentrations in a homogeneously stirred solution of 0.1 M PBS with an applied potential of +0.84 V (Fig. 10). For each addition of NO_2^- with a sample interval of 60 s, a significant current response was observed (Fig. 10A) and it suggests that the rGO-Co_3O_4@Pt efficiently promoted the oxidation of NO in 0.1 M PBS (pH 2.5). The plot of current response versus concentration of NO_2^- showed a linear relation for the concentration range of 10 μM-650 μM (Fig. 10B). Repeated measurements were performed for the detection of NO at lower concentration levels and the current response was reproduced at the nanocomposite modified electrode. The nanocomposite showed the sensitivity of 0.026±0.0002 μA/μM and the limit of detection was calculated as 1.73 μM toward the detection of NO. The comparison of the analytical performance of present rGO-Co_3O_4@Pt nanocomposite modified GC electrode with some of the reported GC electrode based electrochemical sensors toward the detection of NO is shown in Table 1.

Selectivity of the rGO-Co_3O_4@Pt nanocomposite for the detection NO was investigated by injecting various possible physiological interferents in the same homogeneouly stirred PBS containing NO and the change in current response was observed. Figure 11 explains the continuously recorded amperometric i–t curve response for the successive additions of NO_2^- and

interferents in a homogeneously stirred 0.1 M PBS (pH 2.5). The current response of the interferents dopamine, ascorbic acid and uric acid was studied by adding them one by one after the few successive additions of NO_2^- (10 μM) in the same stirred PBS and however, the added interferents did not make any current response even with 100-fold higher concentration. Again the injection of NO_2^- in the same solution displayed almost same magnitude of current response for the oxidation of NO. After the few successive additions of NO_2^-, the more interferents such as glucose, urea and NaCl were added one by one in the continuously recorded i-t curve with a sample of 60 s and the addition of these interferents did not produce enhancement in the current response and however, the introduction of 10 μM NO_2^- to the same solution again resulted in a clear and quick response. These results indicated that the present sensor possesses good selectivity and sensitivity towards the determination of NO_2^- even in the presence of 100-fold excess of common physiological interferents.

Conclusions

We successfully synthesized Co_3O_4@Pt nanocubes incorporated rGO sheets using hydrothermal synthesis. The reduction of GO to rGO was confirmed from the increase in the ratio of D and G bands (I_D/I_G) of Raman spectra. The morphology of Co_3O_4 and the deposition of Pt on Co_3O_4 nanocubes were confirmed by the FESEM analysis and the EDX elemental mapping analysis confirmed the presence of all the elements of the rGO-Co_3O_4@Pt nanocomposite. The rGO-Co_3O_4@Pt nanocomposite modified GC electrode shifted the oxidation overpotential of in-situ generated NO toward less positive potential with enhanced catalytic peak current when compared to the other modified electrodes used in this work. The higher catalytic effect of the rGO-Co_3O_4@Pt nanocomposite was attributed to the synergistic effect of Co_3O_4 nanocubes and Pt nanoparticles present in the rGO matrix. The detection of NO was performed using

amperometric i-t curve technique at the various modified electrodes and among them, the rGO-Co_3O_4@Pt nanocomposite modified electrode showed better performance with lowest detection limit of 1.73 μM. Also, the nanocomposite modified electrode displayed good selectivity toward NO even in the presence of 100-fold higher concentration of other physiologically interested analytes. The current sensor was stable and reproducible and it could add further credits to the rGO-Co_3O_4 nanocomposite based electrochemical sensors in the contemporary research.

Acknowledgement

This work was supported by the High Impact Research Grant from the Ministry of Higher Education of Malaysia (UM.C/625/1/HIR/MOHE/05).

References:

1. Z. H. Taha, *Talanta*, 2003, 61, 3-10.
2. L. J. Ignarro, G. M. Buga, K. S. Wood, R. E. Byrns and G. Chaudhuri, *Proceedings of the National Academy of Sciences*, 1987, 84, 9265-9269.
3. R. F. Furchgott, *Angewandte Chemie International Edition*, 1999, 38, 1870-1880.
4. F. Guix, I. Uribesalgo, M. Coma and F. Munoz, *Progress in neurobiology*, 2005, 76, 126-152.
5. C. X. Guo, S. R. Ng, S. Y. Khoo, X. Zheng, P. Chen and C. M. Li, *ACS nano*, 2012, 6, 6944-6951.
6. F. C. Fang, *Journal of Clinical Investigation*, 1997, 99, 2818.
7. A. Schwentker, Y. Vodovotz, R. Weller and T. R. Billiar, *Nitric oxide*, 2002, 7, 1-10.
8. J.-d. Luo and A. F. Chen, *Acta Pharmacologica Sinica*, 2005, 26, 259-264.
9. C. Bogdan, *Nature immunology*, 2001, 2, 907-916.
10. S. Moncada and A. Higgs, *The New England journal of medicine*, 1993, 329, 2002-2012.
11. E. M. Hetrick and M. H. Schoenfisch, *Annual review of analytical chemistry (Palo Alto, Calif.)*, 2009, 2, 409.
12. B. J. Privett, J. H. Shin and M. H. Schoenfisch, *Chemical Society Reviews*, 2010, 39, 1925-1935.

13. F. Bedioui and N. Villeneuve, *Electroanalysis*, 2003, 15, 5-18.

14. S. Wang and X. Lin, *Electrochimica acta*, 2005, 50, 2887-2891.

15. C. M. Li, J. Zang, D. Zhan, W. Chen, C. Q. Sun, A. L. Teo, Y. Chua, V. Lee and S. Moochhala, *Electroanalysis*, 2006, 18, 713-718.

16. F.-H. Wu, G.-C. Zhao and X.-W. Wei, *Electrochemistry Communications*, 2002, 4, 690-694.

17. Q. He, D. Zheng and S. Hu, *Microchimica Acta*, 2009, 164, 459-464.

18. T. Malinski and Z. Taha, 1992.

19. S. Thangavel and R. Ramaraj, *The Journal of Physical Chemistry C*, 2008, 112, 19825-19830.

20. S. Jayabal, P. Viswanathan and R. Ramaraj, *RSC Advances*, 2014, 4, 33541-33548.

21. Y. Wang, B. Song, J. Xu and S. Hu, *Microchimica Acta*, 2014, 182, 711-718.

22. W. Li, X. Geng, Y. Guo, J. Rong, Y. Gong, L. Wu, X. Zhang, P. Li, J. Xu and G. Cheng, *ACS nano*, 2011, 5, 6955-6961.

23. Y. Zhu, S. Murali, W. Cai, X. Li, J. W. Suk, J. R. Potts and R. S. Ruoff, *Adv Mater*, 2010, 22, 3906-3924.

24. H. Chang and H. Wu, *Energy & Environmental Science*, 2013, 6, 3483-3507.

25. K. S. Kim, Y. Zhao, H. Jang, S. Y. Lee, J. M. Kim, K. S. Kim, J.-H. Ahn, P. Kim, J.-Y. Choi and B. H. Hong, *Nature*, 2009, 457, 706-710.

26. Y.-G. Zhou, J.-J. Chen, F.-b. Wang, Z.-H. Sheng and X.-H. Xia, *Chemical Communications*, 2010, 46, 5951-5953.

27. N. Mahmood, C. Zhang, H. Yin and Y. Hou, *Journal of Materials Chemistry A*, 2014, 2, 15-32.

28. C. Karuppiah, S. Palanisamy, S.-M. Chen, V. Veeramani and P. Periakaruppan, *Sensors and Actuators B: Chemical*, 2014, 196, 450-456.

29. Y. Choi, M. Gu, J. Park, H. K. Song and B. S. Kim, *Advanced Energy Materials*, 2012, 2, 1510-1518.

30. S. Guo, S. Dong and E. Wang, *Acs Nano*, 2009, 4, 547-555.

31. Q. Qu, S. Yang and X. Feng, *Advanced materials*, 2011, 23, 5574-5580.

32. R. Kou, Y. Shao, D. Mei, Z. Nie, D. Wang, C. Wang, V. V. Viswanathan, S. Park, I. A. Aksay and Y. Lin, *Journal of the American Chemical Society*, 2011, 133, 2541-2547.

33. Z. S. Wu, D. W. Wang, W. Ren, J. Zhao, G. Zhou, F. Li and H. M. Cheng, *Advanced Functional Materials*, 2010, 20, 3595-3602.

34. Y. Lu, Y. Wang, Y. Zou, Z. Jiao, B. Zhao, Y. He and M. Wu, *Electrochemistry Communications*, 2010, 12, 101-105.

35. C.-H. Chen, Y.-C. Chen and M.-S. Lin, *Biosensors and Bioelectronics*, 2013, 42, 379-384.

36. J. Mu, L. Zhang, M. Zhao and Y. Wang, *Journal of Molecular Catalysis A: Chemical*, 2013, 378, 30-37.

37. S. Farhadi, K. Pourzare and S. Bazgir, *Journal of Alloys and Compounds*, 2014, 587, 632-637.

38. S. Farhadi, J. Safabakhsh and P. Zaringhadam, *Journal of Nanostructure in Chemistry*, 2013, 3, 1-9.

39. L. Pan, H. Zhao, W. Shen, X. Dong and J. Xu, *Journal of Materials Chemistry A*, 2013, 1, 7159-7166.

40. J. Xiao, Q. Kuang, S. Yang, F. Xiao, S. Wang and L. Guo, *Scientific reports*, 2013, 3.

41. M. M. Lencka, M. Oledzka and R. E. Riman, *Chemistry of materials*, 2000, 12, 1323-1330.

42. N. Huang, H. Lim, C. Chia, M. Yarmo and M. Muhamad, *International journal of nanomedicine*, 2011, 6, 3443.

43. R. Nie, J. Shi, W. Du, W. Ning, Z. Hou and F.-S. Xiao, *Journal of Materials Chemistry A*, 2013, 1, 9037-9045.

44. M. M. Shahid, A. Pandikumar, A. M. Golsheikh, N. M. Huang and H. N. Lim, *RSC Advances*, 2014, 4, 62793-62801.

45. Z. Song, Y. Zhang, W. Liu, S. Zhang, G. Liu, H. Chen and J. Qiu, *Electrochimica Acta*, 2013, 112, 120-126.

46. S.-S. Li, J.-N. Zheng, X. Ma, Y.-Y. Hu, A.-J. Wang, J.-R. Chen and J.-J. Feng, *Nanoscale*, 2014, 6, 5708-5713.

47. Y. Kim, Y. Noh, E. J. Lim, S. Lee, S. M. Choi and W. B. Kim, *Journal of Materials Chemistry A*, 2014, 2, 6976-6986.

48. H. Kim, D.-H. Seo, S.-W. Kim, J. Kim and K. Kang, *Carbon*, 2011, 49, 326-332.

49. H.-C. Liu and S.-K. Yen, *Journal of Power Sources*, 2007, 166, 478-484.

50. J. Jia, B. Wang, A. Wu, G. Cheng, Z. Li and S. Dong, *Analytical Chemistry*, 2002, 74, 2217-2223.

51. J. Rubio-Retama, J. Hernando, B. Lopez-Ruiz, A. Härtl, D. Steinmüller, M. Stutzmann, E. Lopez-Cabarcos and J. Antonio Garrido, *Langmuir*, 2006, 22, 5837-5842.

52. G. Maduraiveeran and R. Ramaraj, *Journal of Electroanalytical Chemistry*, 2007, 608, 52-58.

53. F. Matemadombo and T. Nyokong, *Electrochimica acta*, 2007, 52, 6856-6864.

54. G. Beltramo and M. Koper, *Langmuir*, 2003, 19, 8907-8915.

55. P. K. Rastogi, V. Ganesan and S. Krishnamoorthi, *Journal of Materials Chemistry A*, 2014, 2, 933-943.

56. J.-M. Zen, A. S. Kumar and H.-F. Wang, *Analyst*, 2000, 125, 2169-2172.

57. X. Chen, H-Y. Long, W-L. Wu and Z-S. Yang, *Thin Solid Films*, 2009, 517, 2787–2791.

58. S. Jia, J. Fei, J. Deng, Y. Cai and J. Li, *Sensors and Actuators B*, 2009, 138, 244–250.

59. A. Pandikumar and R. Ramaraj, *Indian Journal of Chemistry*, 2011, 50A, 1388-1393.

60. Y-C. Liu, J. Zhao, W-L. Wu, Z-S. Yang, *Electrochimica Acta*, 2007, 52, 4848–4852.

61. D. Zheng, X. Liu, D. Zhou and S. Hu, *Microchimica Acta*, 2012, 176, 49–55.

62. S. L. Ting, C. X. Guo, K. C. Leong, D-H Kim, C. M. Li and P. Chen, *Electrochimica Acta*, 2013, 111, 441–446.

63. J. Fei, S. Hu and K-K. Shiu, *Journal of Solid State Electrochemistry*, 2011, 15, 519–523.

64. N. Yusoff, A. Pandikumar, A. R. Marlinda, N. M. Huang and H. N. Lim, *Analytical Methods*, 2015, 7, 3537-3544.

65. X. He and L. Zhu, *Electrochemistry Communications*, 2006, 8, 615–620.

Table 1 Comparison of some of the reported electrochemical sensors for NO detection.

Modified GC electrode[a]	Technique[b]	pH	Linear range	LOD (μM)	Reference
GC/PAM/SDS/Cyt c	Amperometry	7.0	0.80 μM– 95 μM	0.1	57
GC/PNMP-b-PGMA/Hb	DPV	7.0	0.45 μM–10 μM	0.32	58
GC/EDAS(TiO_2-Au)$_{nps}$	SWV	2.5	1 μM– 60 μM	1.0	59
GC/DNA/Cyt c	Amperometry	5.0	0.6 μM– 8 μM	0.1	60
GC/PtNP/AB	Amperometry	7.4	0.18 μM– 120 μM	0.05	61
GC/AuNP-ERGO	Amperometry	7.4	up to 3.38 μM	0.133	62
GC/SWNT/PVP–Os–EA	Amperometry	7.4	0.2 μM– 40 μM	0.05	63
GC/G-Nf	SWV	2.5	50 μM– 450 μM	11.61	64
GC/Hb–CPB/PAM	CV	4.42	9.8 μM– 100 μM	9.3	65
GC/rGO-Co_3O_4@Pt	Amperometry	2.5	10 μM– 650 μM	1.73	Present work

[a] PAM = polyacrylamide; SDS = sodium dodecyl sulfate; Cyt c = cytochrome c; PNMP-b-PGMA = poly [N-(2-methacryloyloxyethyl) pyrrolidone]-blockpoly [glycidyl methacrylate]; Hb = hemoglobin; EDAS = N-[3-(trimethoxysilyl)propyl]ethylene diamine; TiO_2-Au = titanium dioxide-gold nanocomposite; DNA = deoxyribonucleic acid; PtNP = platinum nanoparticle; AB = acetylene black; AuNP = gold nanoparticle; ERGO = electrochemically reduced graphene oxide; SWNT = single-walled carbon nanotube; PVP–Os–EA = Os-bipyridine complex and poly(4-vinylpyridine) (PVP) partially quaternized with 2-bromoethylamine (EA) functionalities; G = graphene; Nf = Nafion; Hb-CPB = hemoglobin-cetylpyridinium bromide. [b] DPV = differential pulse voltammetry; SWV = square wave voltammetry; CV = cyclic voltammetry.

Figures and Caption

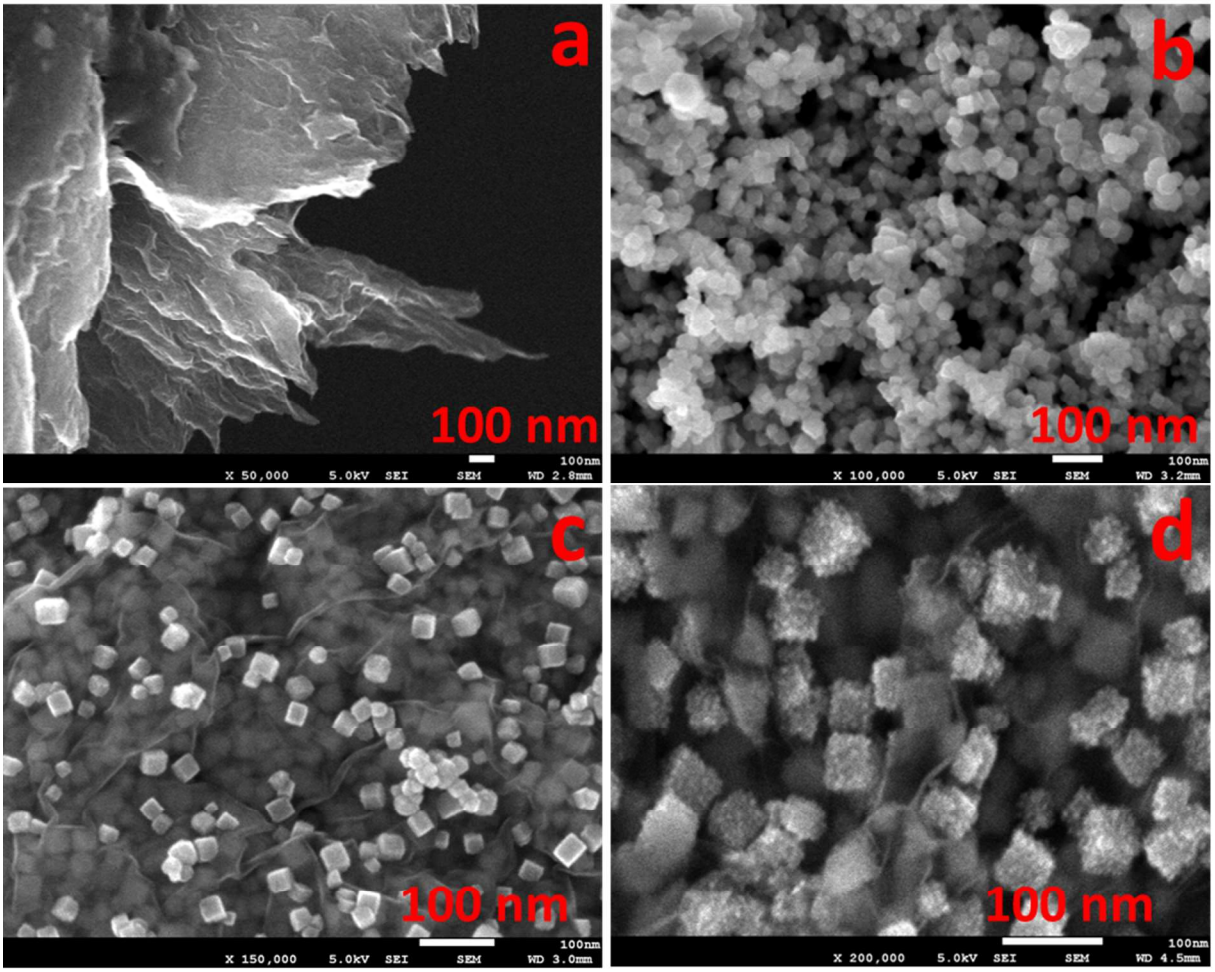

Fig. 1 FESEM images of rGO sheets (a), Co_3O_4 nanocubes (b), rGO-Co_3O_4 nanocomposite (c) and rGO-Co_3O_4@Pt nanocomposite (d).

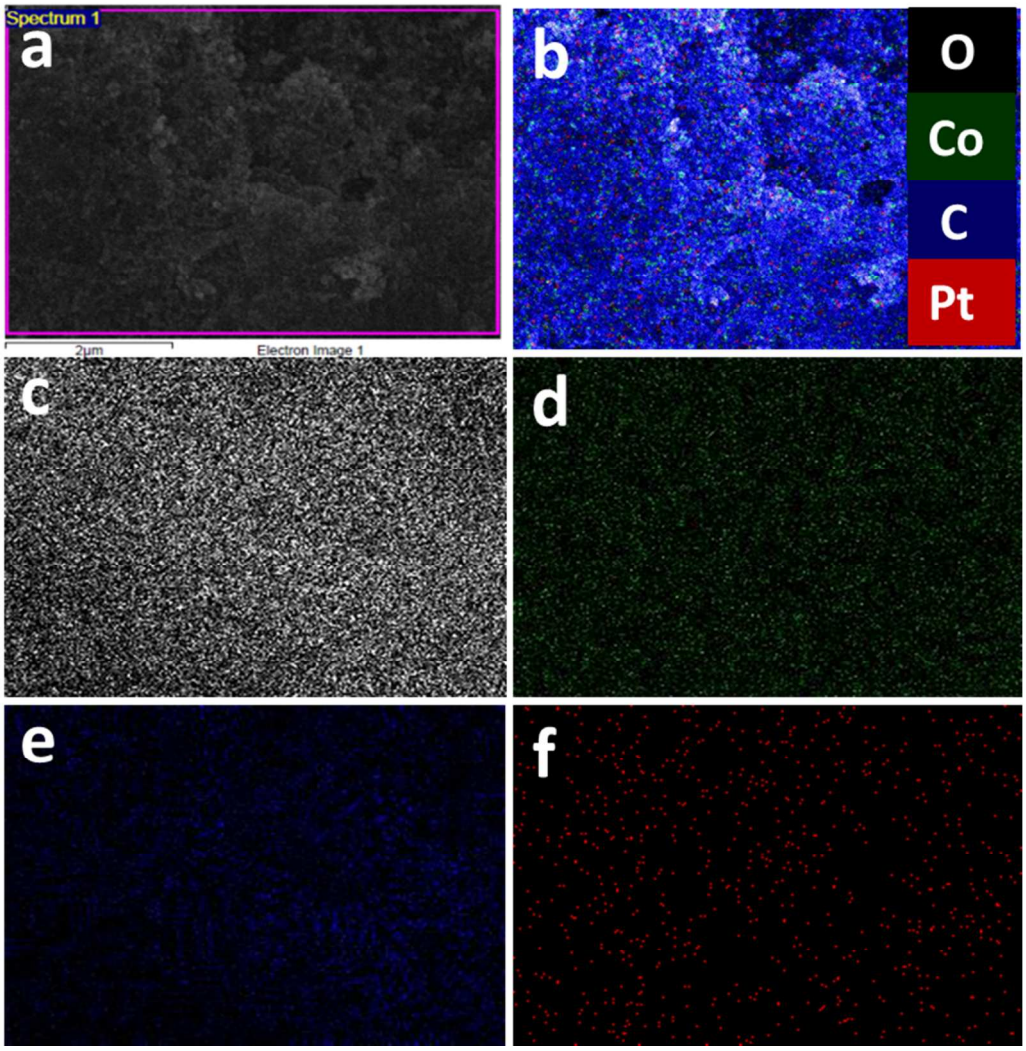

Fig. 2 FESEM image (a) and EDX elemental mapping (b) of rGO/Co_3O_4@Pt nanocomposite: black (c), green (d), blue (e) and red (f) corresponding to the elements O, Co, C and Pt, respectively.

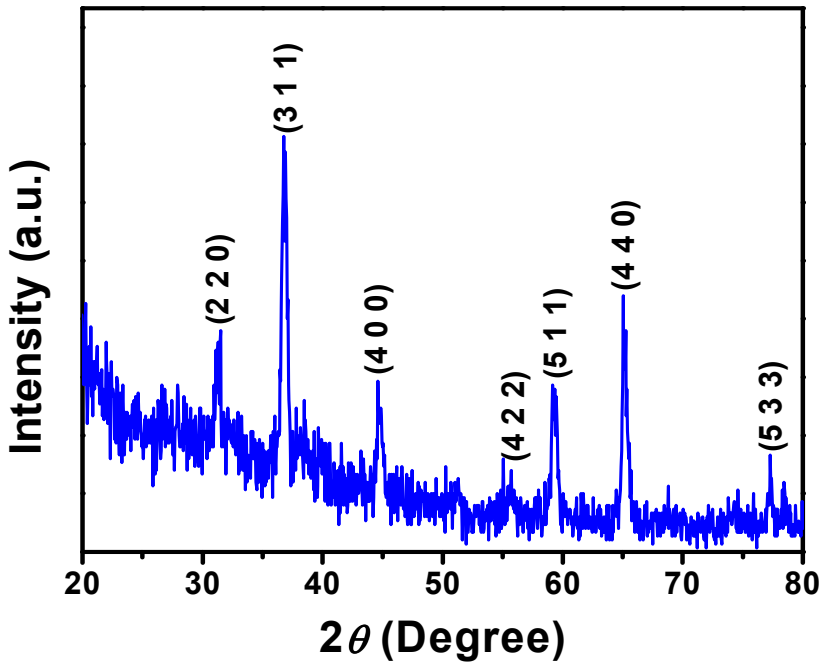

Fig. 3 XRD pattern of rGO-Co_3O_4@Pt nanocomposite.

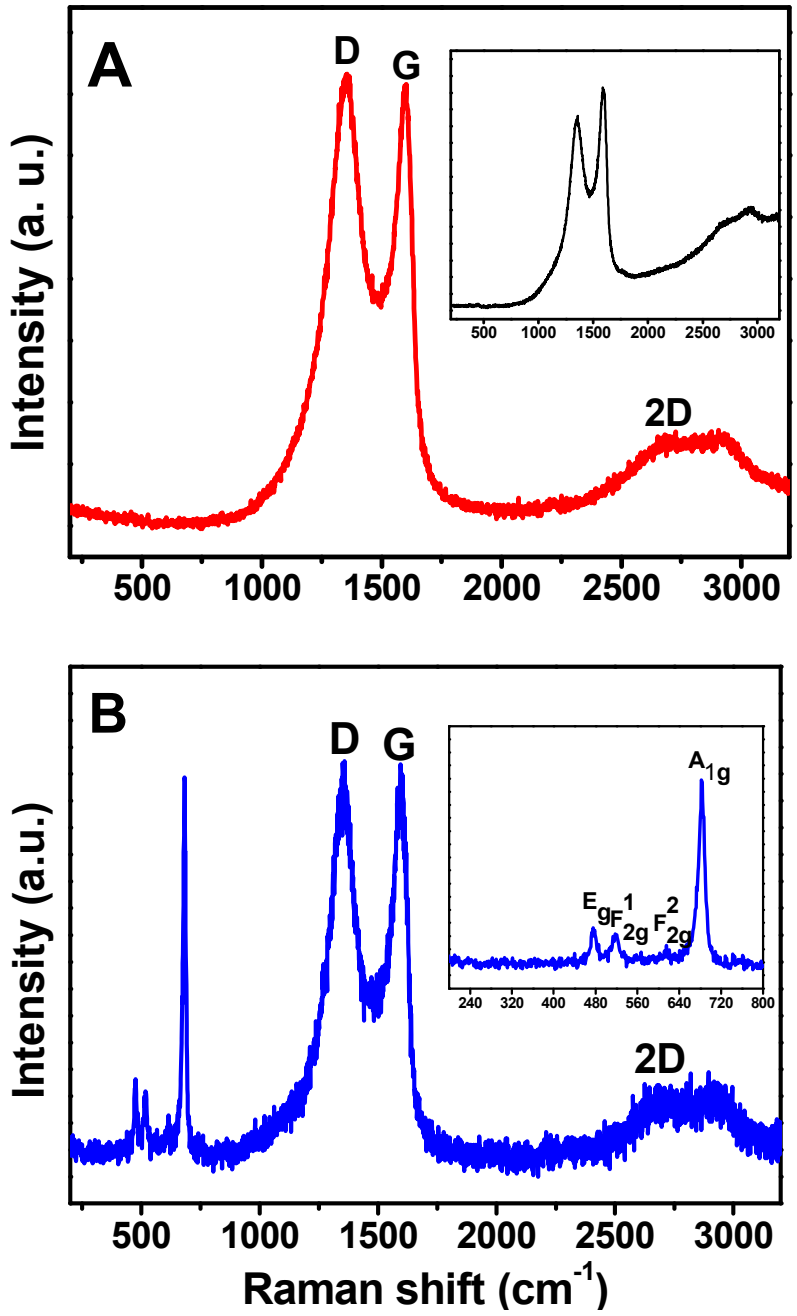

Fig. 4 Raman spectra of rGO sheet (Inset: Raman spectrum of GO sheet) (A) and rGO-Co_3O_4@Pt nanocomposite (Inset: expanded view of Raman modes of Co_3O_4) (B).

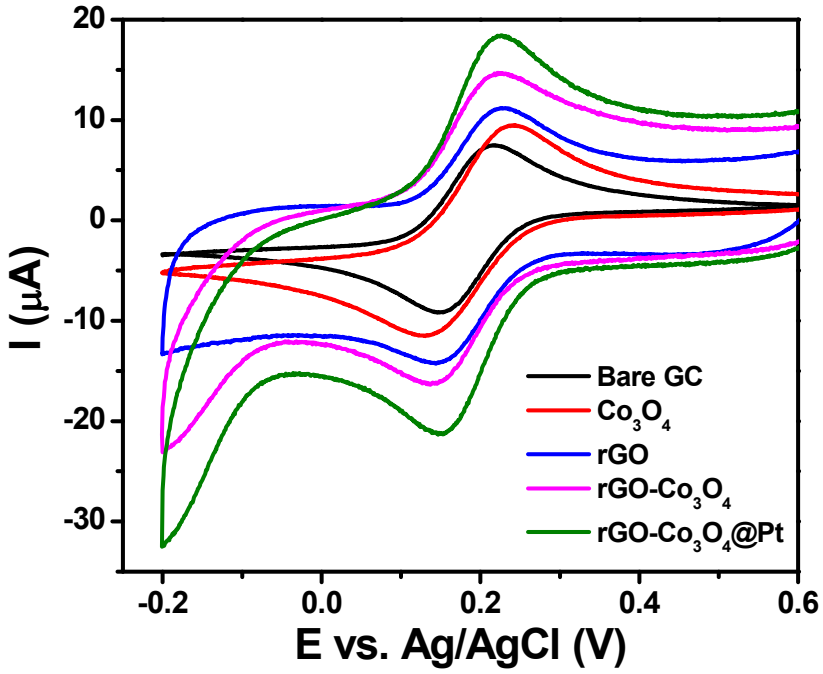

Fig. 5 Cyclic voltammograms obtained for Bare GC, Co_3O_4 nanocubes, rGO, rGO-Co_3O_4 nanocomposite and rGO-Co_3O_4@Pt nanocomposite modified GC electrodes for 1 mM $K_3[Fe(CN)_6]$ in 0.1 M KCl at a scan rate of 50 mV s^{-1}.

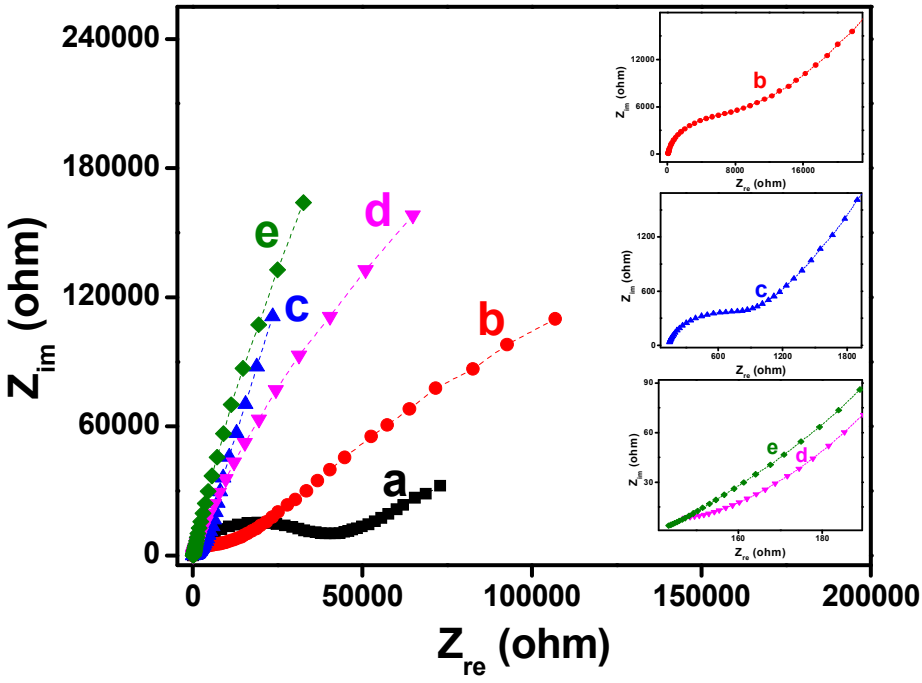

Fig. 6 Nyquist plots obtained for bare GC (a) Co_3O_4 nanocubes (b), rGO (c), rGO-Co_3O_4 nanocomposite (d) and rGO-Co_3O_4@Pt nanocomposite (e) modified GC electrodes for 1 mM $K_3[Fe(CN)_6]$ in 0.1 M KCl. The frequency range was 0.01 Hz to 10 kHz.

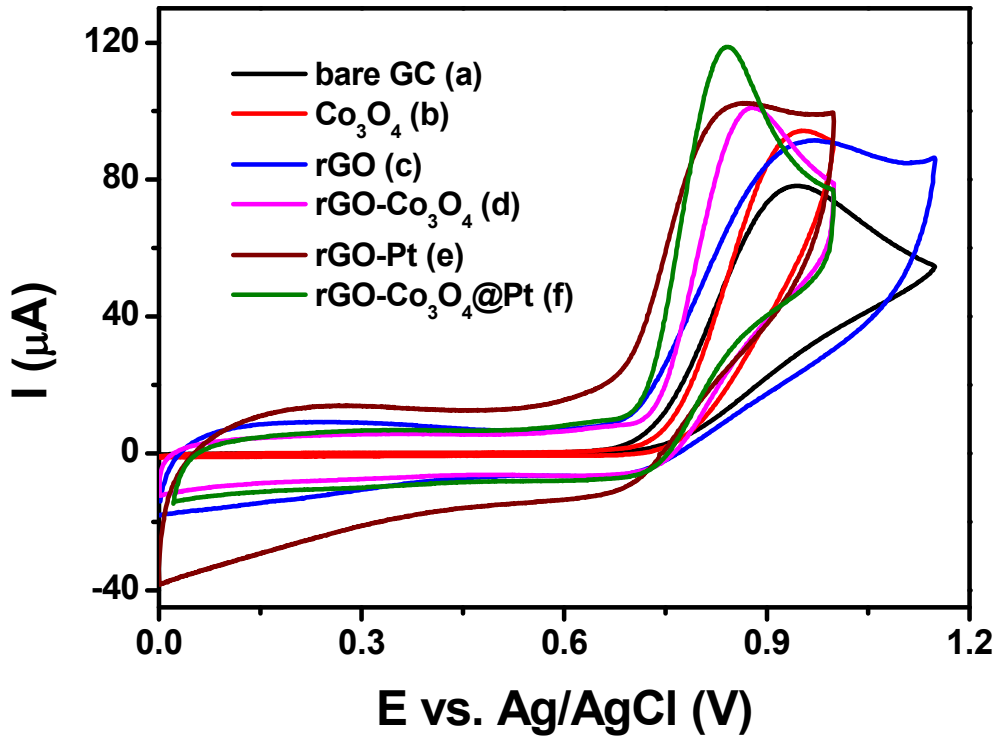

Fig. 7 Cyclic voltammograms recorded at bare GC (a), Co_3O_4 nanocubes (b), rGO (c), rGO-Co_3O_4 nanocomposite (d), rGO-Pt nanocomposite (e) and rGO-Co_3O_4@Pt nanocomposite (f) modified electrodes for 5 mM of NO_2^- in 0.1 M PBS (pH 2.5) with a scan rate of 50 mVs^{-1}.

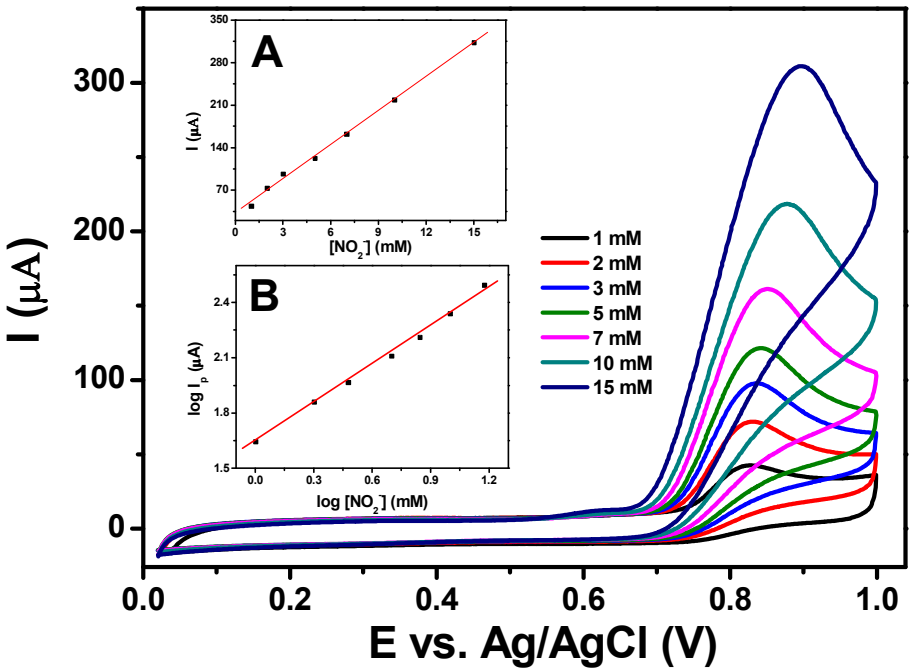

Fig. 8 Cyclic voltammograms obtained at rGO-Co_3O_4@Pt nanocomposite modified electrode during successive addition of different concentrations of NO_2^- in 0.1 M PBS (pH 2.5) with a scan rate of 50 mVs^{-1}.

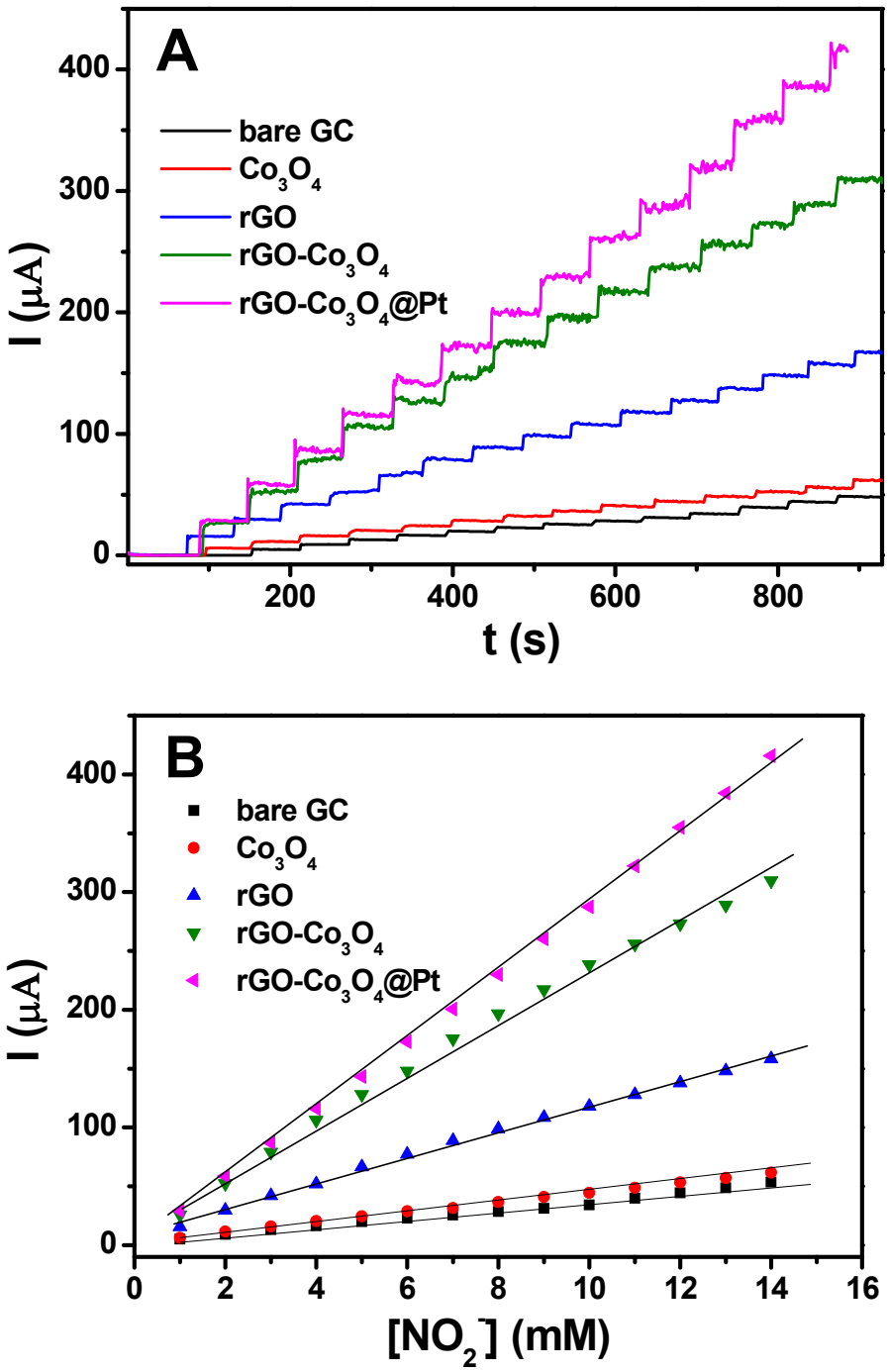

Fig. 9 Amperometric i–t curves obtained at bare GC, Co_3O_4 nanocubes, rGO, rGO-Co_3O_4 nanocomposite and rGO-Co_3O_4@Pt nanocomposite modified GC electrodes for the successive addition of 1 mM NO_2^- in 0.1 M PBS (pH 2.5) at a regular interval of 60 s (A) and corresponding

calibration plots of current versus concentration of NO_2^- (B). Applied potentials were the peak potentials obtained from Fig. 7.

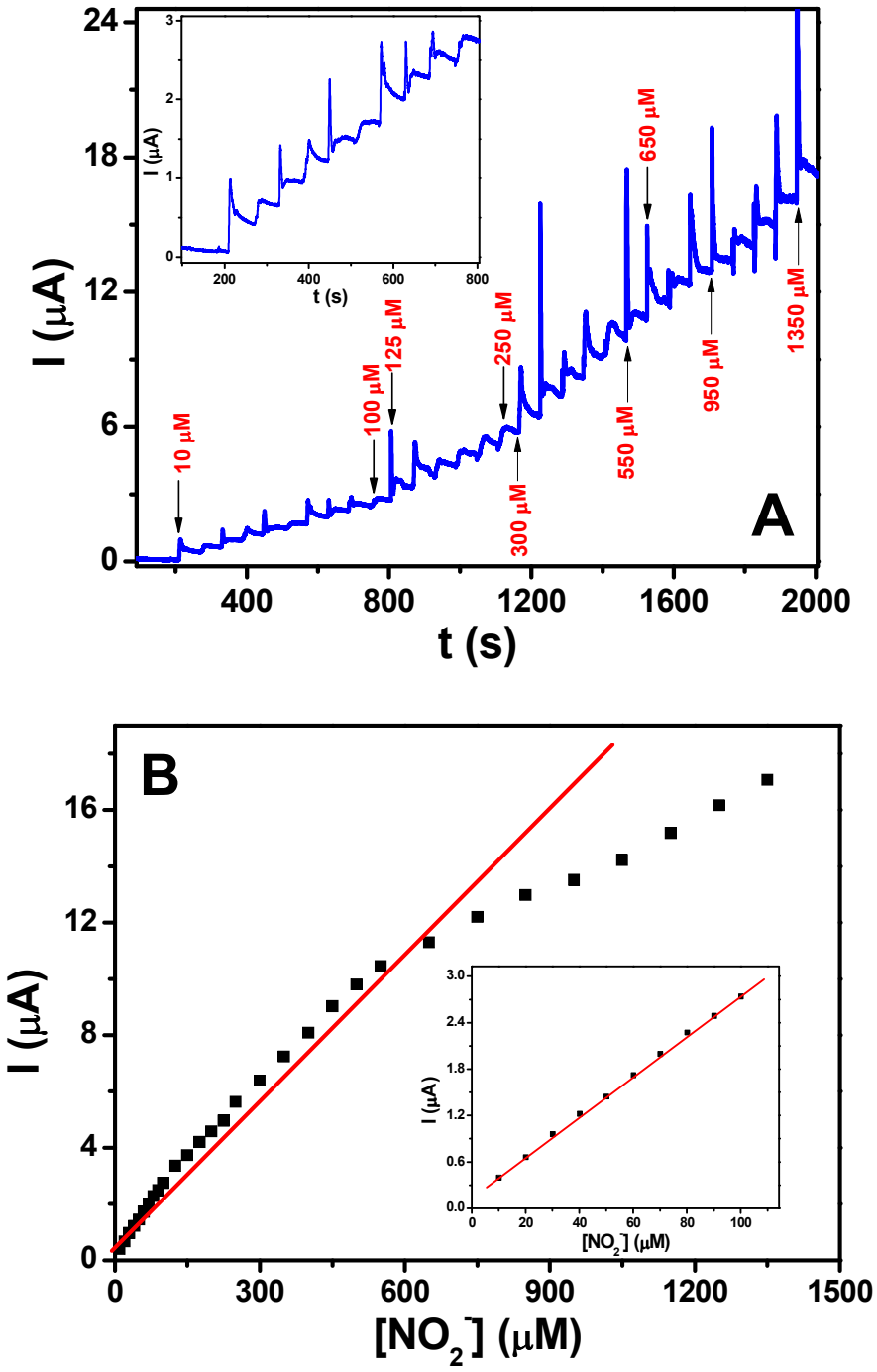

Fig. 10 A) Amperometric i–t curves obtained at rGO-Co_3O_4@Pt nanocomposite modified GC electrodes for the successive addition of NO_2^- with various concentrations in 0.1 M PBS (pH 2.5)

at a regular interval of 60 s. Inset: expanded view of i–t curve obtained for the successive addition of 10 μM NO_2^-. Applied potential was +0.84 V. B) Calibration plot of peak current versus concentration of NO_2^- corresponding to 'A'. Inset: expanded view of linear calibration plot corresponding to 10 μM NO_2^- addition.

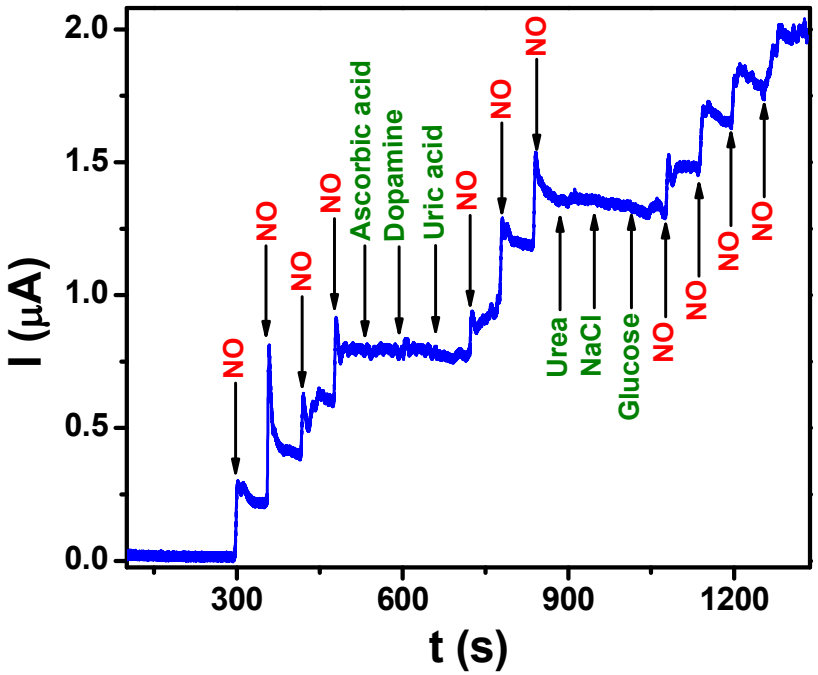

Fig. 11 Amperometric i–t curve obtained at rGO-Co_3O_4@Pt nanocomposite modified GC electrode for the successive addition of 10 μM NO_2^- and each 1 mM of dopamine, ascorbic acid, uric acid, glucose, urea and NaCl in 0.1 M PBS (pH 2.5) at a regular interval of 60 s. Applied potential was +0.84 V.